ELSEVIER

Chemical Geology 211 (2004) 343–362

CHEMICAL GEOLOGY
INCLUDING
ISOTOPE GEOSCIENCE

www.elsevier.com/locate/chemgeo

Experimental determination of Fe isotope fractionation between aqueous Fe(II), siderite and "green rust" in abiotic systems

René A. Wiesli*, Brian L. Beard, Clark M. Johnson

Department of Geology and Geophysics, University of Wisconsin, Lewis G. Weeks Hall, 1215 W. Dayton St., Madison, WI 53706 USA

Received 30 December 2003; accepted 16 July 2004

Abstract

Iron isotope fractionation between aqueous iron and siderite has been measured using abiotic synthesis experiments at ~20 °C. Applying a Rayleigh distillation model to three experiments in which siderite ($FeCO_3$) was continuously precipitated from solutions over the course of tens of hours, the derived fractionation factor is $10^3 \ln\alpha_{Fe(II)-Siderite} = +0.48 \pm 0.22‰$ (2σ). This experimentally determined fractionation factor is significantly smaller (by ~1.5‰) than that calculated from vibrational frequencies and Mössbauer shifts [Geochim. Cosmochim. Acta 64 (2000) 849–865; Geochim. Cosmochim. Acta 65 (2001) 2487–2497], and lies on the high end of that inferred from natural mineral assemblages, where the $Fe(II)_{aq}$–siderite fractionation factor was inferred to lie between −1.7‰ and +0.3‰ [Contrib. Mineral. Petrol. 144 (2003) 523–547]. The measured $Fe(II)_{aq}$–siderite fractionation from this study suggests that siderite from Archean and Proterozoic rocks, which have moderately negative δ^{56}Fe values (−1.5‰ to −0.5‰), may reflect precipitation from $Fe(II)_{aq}$ whose origin was hydrothermal. In contrast, natural siderites that have higher δ^{56}Fe values apparently require non-hydrothermal sources of Fe and/or different pathways of formation, or may reflect the effects of cation substitution on the $Fe(II)_{aq}$–carbonate fractionation factor.

Keywords: Iron-isotopes; Isotope fractionation; Siderite; Green rust

1. Introduction

Iron isotope compositions from a variety of geologic materials record a range of ~4‰ in $^{56}Fe/^{54}Fe$ ratios (e.g., Beard and Johnson, 1999; Zhu et al., 2000; Zhu et al., 2001; Johnson et al., 2003; Beard and Johnson, 2004). The origin of naturally occurring Fe isotope variations is not completely clear because there is not a significant data base of well-known isotopic fractionation factors, as there is for more common isotope systems such as C, O and S. However, work to date has demonstrated that at low temperatures, redox changes in both biologic and abiologic systems produce some of the largest Fe isotope variations (Beard et al., 1999;

* Corresponding author. Tel.: +1 608 262 8960; fax: +1 608 262 0693.
E-mail address: renew@geology.wisc.edu (R.A. Wiesli).

0009-2541/$ - see front matter © 2004 Elsevier B.V. All rights reserved.
doi:10.1016/j.chemgeo.2004.07.002

Bullen et al., 2001; Matthews et al., 2001; Johnson et al., 2002; Beard et al., 2003a; Welch et al., 2003; Croal et al., 2004; Johnson et al., 2004). In addition, experimental studies have documented Fe isotope fractionations produced on ion-exchange columns (Anbar et al., 2000; Roe et al., 2003), as well as during mineral dissolution in the presence of organic ligands (Brantley et al., 2001). Fluid–mineral fractionations are particularly important to determine so that the Fe isotope compositions of ancient Fe-bearing fluids may be inferred from the rock record. So far, equilibrium fluid–mineral fractionations for Fe have only be determined for the system $Fe(III)_{aq}$–hematite (Skulan et al., 2002).

Iron-bearing carbonates such as siderite and ankerite are common in the rock record (e.g., Klein and Beukes, 1992), and are found in rocks of Archean to modern age (Postma, 1982; Curtis et al., 1986; Pye et al., 1990; Mozley and Carothers, 1992; Raiswell and Fisher, 2000; Uysal et al., 2000; Hendry, 2002). In biologic experiments using a dissimilatory Fe(III)-reducing bacteria (*Shewanella putrefaciens*, strain CN32) and ferrihydrite as the substrate, Johnson et al. (2004) estimate that the equilibrium fractionation between $Fe(II)_{(aq)}$ and precipitated siderite ($FeCO_3$) is approximately zero. In contrast, $Fe(II)_{aq}$–siderite fractionations inferred from natural assemblages such as banded iron formations span a range between −1.7‰ and +0.3‰ (Johnson et al., 2003). Large equilibrium iron isotope fractionations between aqueous Fe and siderite (~2‰ at room temperature) have also been predicted from spectroscopic data (Polyakov, 1997; Polyakov and Mineev, 2000; Schauble et al., 2001). However, these fractionations have not been confirmed in experimental systems.

Here, we report the results of experiments that constrain the equilibrium Fe isotope fractionation between aqueous Fe(II), siderite and "green rust". In addition to its common occurrence in a variety of modern and ancient environments, diagenetic siderite concretions have been interpreted to reflect microbially mediated reactions (e.g., Curtis et al., 1986) and may be a natural analogue to siderite precipitated in experiments employing dissimilatory Fe(III) reducing bacteria (Johnson et al., 2004). "Green rusts" are metastable, mixed Fe^{II}–Fe^{III} hydroxy compounds which have been found in anoxic soils (Trolard et al., 1997), and as a corrosion product of steel under anoxic conditions (e.g., Stampfl, 1969; Abdelmoula et al., 1996). In addition, "green rust" has been identified as a product in dissimilatory Fe(III) reducing experiments (Fredrickson et al., 1998; Parmar et al., 2002). A general formula for "green rusts" is $[Fe^{II}_a Fe^{III}_b (OH)_x][A_{(2a+3b-x)/z}] \cdot nH_2O$, where A is an interlayer anion with valence z (Lewis, 1997). The structure of "green rust" is made up of sheets of $Fe(OH)_6$ octahedra in which some of the Fe^{II} is replaced by Fe^{III}. The resulting positive layer charge is compensated by interlayer anions like including Cl^-, SO_4^{2-}, CO_3^{2-}, OH^- and ClO_4^-. Reported Fe^{II}/Fe^{III} ratios in "green rusts" range from 0.8 to 3.6 (Cornell and Schwertmann, 2003).

Synthesis experiments were employed using reagents ferrous perchlorate ($Fe(ClO4)_2 \cdot 6H_2O$) and sodium bicarbonate ($NaHCO_3$) to precipitate siderite and "green rust". Although the main emphasis of this study is on the Fe isotope fractionation in the $Fe(II)_{aq}$–siderite system, a short assessment of Fe isotope fractionation in the mixed Fe^{II}–Fe^{III}–"green rust" system is also given. Rates of precipitation were varied for different experiments, and the Fe isotope composition of different size fractions of siderite and "green rust" were measured to understand the pathways involved in producing the measured isotopic fractionations.

2. Experimental methods

The goal of the experiments was to determine the equilibrium Fe isotope fractionation between hexaaquo Fe(II) and siderite at low temperatures. Because perchlorates are a weak ligand (e.g., Johansson and Yokohama, 1990), we expect the dominant aqueous Fe species to be $[Fe^{II}(H_2O)_6]^{2+}$, allowing direct comparison with the predicted $[Fe^{II}(H_2O)_6]^{2+}$–$FeCO_3$ fractionations of Polyakov and Mineev (2000) and Schauble et al. (2001). Use of $FeCl_2$ as the initial Fe reagent would add additional uncertainty in the nature of the aqueous Fe species, although it appears that at least in the case of ferric Fe species, chloride substitution up to the monochloro complex produces insignificant Fe isotope effects (Welch et al., 2003).

Rigorous demonstration of attainment of isotopic equilibrium at low temperatures is difficult or even impossible due to the slow rates of isotopic exchange in

solids at low temperature, requiring mineral synthesis experiments to investigate fluid–mineral fractionation factors (O'Neil, 1986; Chacko et al., 2001). Unidirectional processes such as precipitation from an aqueous solution may produce kinetic isotope fractionation, although it is generally expected that the measured fractionations will approach equilibrium fractionations as rates of precipitation approach zero, and this is the approach that was followed in the current study (e.g., Carothers et al., 1988; Kim and O'Neil, 1997; Bao and Koch, 1999; Skulan et al., 2002).

2.1. Synthesis of siderite

The siderite synthesis experiments were carried out in a 250-ml glass reaction vessel that contained multiple ports, which allowed introduction of gases and periodic sampling through a rubber septum. All solutions were made with anaerobic 18 MΩ water obtained by boiling 18 MΩ water for ~1 h with continuous flushing by Ar or N_2. For a typical experiment, the reaction vessel was filled with 150 ml of a bicarbonate solution (0.02–0.33 mol/l), which was flushed for several hours with CO_2 gas to lower the pH to ~4. After checking the pH (~4), 50 ml of oxygen-free, ferrous perchlorate solution (0.02–0.5 mol/l) was added to the reaction vessel at a rate of 0.16 ml/min using a peristaltic pump. Following introduction of ferrous perchlorate, CO_2 was slowly replaced by a controlled flow of a Ar/H_2 (95:5) mixture, where the rate was controlled by a flow meter at ~3 ml/min. Replacing $CO_2$with Ar/H_2 increased the pH of the solution and consequently induced precipitation. Depending on the concentrations of reagents used, precipitation started immediately or was delayed until sufficient supersaturation was attained. Sample suspensions (liquid and precipitate) were extracted with a 10-ml syringe through a rubber septum and transferred to an anaerobic glove box that contained an Ar atmosphere for further processing. Precipitates were filtered first through a 10-μm filter, followed by filtration through a 0.22-μm (or 0.45 μm) filter (PTFE membranes from *Osmonics*). Filtrates were washed with deoxygenated water. Some filtrate was set aside to dry to be used for scanning electron microscope (SEM) and X-ray diffraction (XRD) analysis, and all the remaining material was dissolved in 0.5 M HCl. Total Fe and Fe(II) contents of solution and dissolved precipitate were determined using the colometric *Ferrozine* method (Dawson and Lyle, 1990). Separate 0.5 M HCl aliquots were processed for Fe isotope analysis.

The morphology and identity of the precipitated phases were investigated using XRD and SEM. SEM images (Fig. 1) indicate that botryoidal (globular) aggregates of carbonate (size range from ~1–10 μm in diameter) were common. The surface of these aggregates from earlier time periods (2.5 h) consisted of rounded spherical particles that protrude from the surface (Fig. 1A). The surface in samples from later time periods (6.25 h and later) appears crystalline, and consisted of submicron-sized cubes that protruded from the surface, possibly reflecting Ostwald ripening (Fig. 1B). X-ray diffraction patterns of the precipitates illustrated in Fig. 1A, B and C confirm that siderite was the only detectable solid phase in these samples, despite their different morphologies.

2.2. Partial dissolution experiments

To test for isotopic heterogeneity in the solid phases, solid run products were partially dissolved in 1 ml of 0.1 mol/l HCl for 5 or 10 min. Strong isotopic zonations or heterogeneities in the solid phases may indicate kinetic isotopic fractionation (Skulan et al., 2002). Before separation of the solid phase, the solutions were centrifuged for ~3 min. The extent of dissolution was determined by measuring Fe concentrations using *Ferrozine* (Dawson and Lyle, 1990) and comparing it to the initial solid weight.

2.3. Iron isotope measurements

All Fe isotope compositions were measured using the University of Wisconsin-Madison *IsoProbe*, a multicollector, inductively coupled plasma-mass spectrometer (MC-ICP-MS). Chemical separation and mass analysis procedures followed the methods of Skulan et al. (2002) and Beard et al. (2003a). Based on replicate analyses of samples and ultrapure Fe standards, the long-term *external* reproducibility for the $^{56}Fe/^{54}Fe$ ratio is ±0.05‰ (1 S.D.). Analyes are reported using delta notation, where $\delta^{56}Fe=10^3([^{56}Fe/^{54}Fe]_{Sample}/[^{56}Fe/^{54}Fe]_{Terr\ Ig\ rocks}-1)$ and $\delta^{57}Fe=10^3([^{57}Fe/^{54}Fe]_{Sample}/[^{57}Fe/^{54}Fe]_{Terr\ Ig\ rocks}-1)$; the reference reservoir of terrestrial igneous rocks likely reflects that of bulk Earth (Beard et al.,

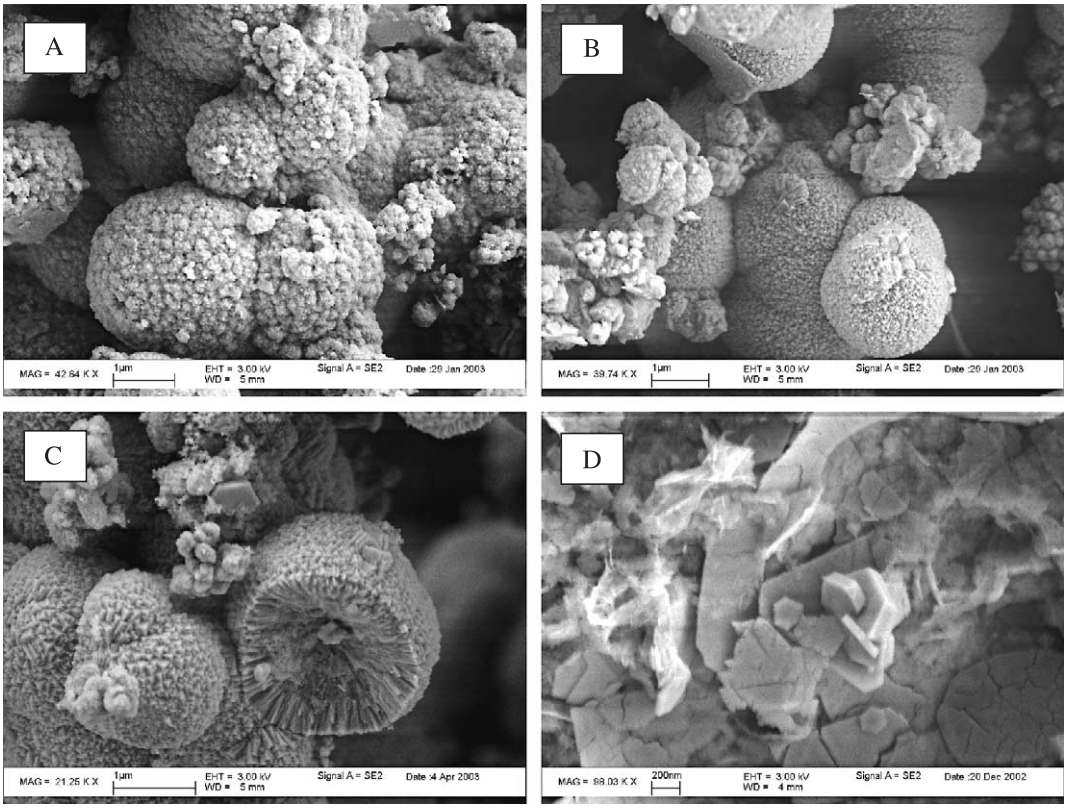

Fig. 1. SEM images of precipitates of Experiments 1 and 2. (A) Precipitate of siderite sampled at 2.5 h after initial precipitation (Experiment 2). The surfaces of the siderite spherules appear non-crystalline. (B) Precipitate of siderite spherules sampled at 6.25 h after initial precipitation (Experiment 2). The surfaces of the siderite spherules consist of small euhedral cubes. (C) Cross-section through a siderite spherule harvested at 49 h (Experiment 2). The spherule consists of radially orientated acicular crystals, possibly elongated in the *c*-axis direction, with euhedral faces at the tip of the acicular crystals (exposed at the surface of the siderite spherules). (D) Hexagonal platelets in Experiment 1, which are likely to be a mixed Fe(II)–Fe(III) phase such as "green rust" (Cornell and Schwertmann, 2003).

2003a). On this scale, the measured Fe isotope composition of the IRMM-014 Fe isotope standard was $\delta^{56}Fe = -0.09 \pm 0.05‰$ and $\delta^{57}Fe = -0.11 \pm 0.07‰$.

3. Results

The extent of Fe isotope fractionation between aqueous Fe(II) and precipitated siderite was investigated using different initial $Fe(II)_{aq}$ concentrations, as well as different Fe/carbonate ratios. It is anticipated that the experiments with slower precipitation rates are more likely to reflect equilibrium conditions. Overall, the measured Fe isotope compositions follow Rayleigh fractionation trends, as is generally expected for precipitation experiments. The instantaneous isotope composition of aqueous Fe(II) using a Rayleigh equation is given by

$$\delta^{56}Fe_{\text{liq. instant.}} = \left[(1000 + \delta^{56}Fe_{\text{liq. initial.}})\ F^{(\alpha-1)}\right] - 1000 \quad (1)$$

where α is the fractionation factor defined as

$$\alpha_{A-B} = \left(^{56}Fe/^{54}Fe\right)_A / \left(^{56}Fe/^{54}Fe\right)_B = \left(\frac{1000 + \delta^{56}Fe_A}{1000 + \delta^{56}Fe_B}\right) \quad (2)$$

and $\delta^{56}Fe_{\text{liq. initial}}$ is the initial isotope composition of $Fe(II)_{aq}$ and F is the fraction of $Fe(II)_{aq}$ remaining in

solution. The isotopic fractionation factor α between siderite and $Fe(II)_{aq}$ can be obtained by linear regression of a plot of Log[F] versus Log[$(1000+\delta^{56}Fe)/(1000+\delta^{56}Fe_i)$] where the slope of the regression line represents $(\alpha-1)$. The average isotope composition of the accumulated siderite is given by

$$\delta^{56}Fe_{Sid.average} = \left[\left\{\frac{1-F^{\alpha}}{1-F}\right\}(1000+\delta^{56}Fe_{liq.\ initial})\right] - 1000 \quad (3)$$

A summary of experimental conditions is given in Table 1. Results of experiment 1, which likely produced a mixed "green rust"–siderite precipitate, is presented first. The results of experiments that involved rapid or slow precipitation rates of siderite will be discussed next. Formation of "green rust" requires the presence of oxygen in aqueous Fe(II) solutions. At the conditions of experiment 1 (pH~4–7, low concentrations of $Fe(II)_{aq}$, bicarbonate and traces of oxygen present; Table 1), "green rust" is a likely precipitate, as has been shown in several experimental studies (e.g., Misawa et al., 1973; Schwertmann and Thalmann, 1976; Legrand et al., 2000). More rigorous exclusion of oxygen from the experiments, in addition to using higher concentrations of Fe(II) and bicarbonate, always resulted in siderite as the main precipitation product (Experiments 2, 3 and 4).

Ferrous and total Fe contents of the solid run products were made using *Ferrozine* assays (Dawson and Lyle, 1990) to check for oxidation of aqueous Fe or the fine-grained solids that may occur if oxygen was present during the experiment or subsequent processing of the samples in the glove box. Oxidation of run products (either aqueous Fe or solid) may compromise the isotopic results, given the large fractionation between ferric and ferrous Fe at room temperature (Johnson et al., 2002; Welch et al., 2003). Some of the low Fe(II)/Fe(tot) ratios reflect oxidation of $Fe(II)_{aq}$ either in the reaction vessel, or later during processing of an extracted suspension in the glove box. In particular, the finer sized fraction of a precipitate is extremely susceptible to oxidation as it changes color (from greenish-gray to orange) within seconds after filtration. Oxidation is more pronounced during the early time points since the smaller size fraction makes up a larger proportion of the solid precipitate. It is important to note, however, that any oxidation that occurs after the solids are separated

Table 1
Summary of experimental conditions

Exp.	Goal	Method	Amount of $NaHCO_3$ used (mol)	Amount of $Fe(ClO_4)_2 \cdot 6H_2O$ (mol)	Initial $[Fe_{aq}]$ (μg)	Final $[Fe_{aq}]$ (μg)	Run time (h)	Rate constants[a] (h^{-1})
1	Measure Fe isotope fractionation during green rust precipitation	Fe into bicarbonate (fast addition, 10 s)	0.003	0.001	56,000	5900	24[b]	−0.0669 (1st order)
2	Measure Fe isotope fractionation during rapid siderite precipitation	Fe into bicarbonate (pump rate=0.16 ml/min)	0.05	0.025	0	0	10.25	6.9714 (2nd order)
3	Measure Fe isotope fractionation during slow siderite precipitation	Fe into bicarbonate (pump rate=0.16 ml/min) (method 1)[c]	0.01	0.01	0	189,000	24.5	0.0646 (2nd order)
4	Measure Fe isotope fractionation during slow siderite precipitation	Bicarbonate into Fe (pump rate=0.16 ml/min) (method 2)[c]	0.01	0.013	720,000	270,000	48	0.0692 (2nd order)

[a] Rate constants have been calculated for comparative purpose only; no specific reaction mechanisms are implied; rate law order noted in parentheses.

[b] Actual run time was 24 h but $Fe(tot)_{aq}$ was at the detection limit for *Ferrozine* (1 ppm) at 12 h.

[c] Method 1 involved the pumping of ferrous perchlorate solution at a rate of 0.16 ml/min into the bicarbonate solution, whereas method 2 involved the pumping of bicarbonate solution into the ferrous perchlorate solution at a rate of 0.16 ml/min.

from the aqueous phase will not affect the isotopic compositions of the solids; the solid products, in fact, are quantitatively converted to aqueous ferric Fe during dissolution in HCl and evaporation prior to purification of Fe from the matrix on anion-exchange columns.

There are potential isotopic effects due to speciation of aqueous Fe in solution (Schauble et al., 2001). Although the initial ferrous perchlorate is not likely to form Fe(II)-perchlorate complexes due to the weakness of the ClO_4^- ligand in dilute aqueous solutions (e.g., Johansson and Yokohama, 1990), mixing with carbonate solutions may form Fe(II)-carbonate complexes such as $Fe(CO_3)_2^{2-}$, $FeCO_3^{\circ}(aq)$ and $FeH(CO_3)^+$. Although speciation calculations (Table 2) indicate that $[Fe^{II}(H_2O)_6]^{2+}$ and $Fe^{II}H(CO_3)^+$ are the dominant Fe species in the initial phase of the experiments (pH~4), replacement of CO_2 through addition of the Ar–H_2 mixture increases the pH of the solution to initiation of siderite precipitation. In addition, $Fe(II)_{aq}$ may also hydrolyze to mononuclear species such as $FeOH^+$ and $Fe(OH)_4^{2-}$ upon increases of pH. Speciation calculations, however, indicate that the concentrations of ferrous hydroxide species are low in comparison to Fe–carbonate complexes (Table 2). It seems likely that polynuclear species of ferrous iron at the Fe concentrations used are not important (Baes and Mesmer, 1976). We do not expect significant isotopic effects due to variations in ferrous hydroxide species because H_2O and OH^- provide virtually identical ligand fields, and this is supported by the relatively constant isotopic fractionation measured between aqueous ferric and ferrous Fe over a wide range of hydroxide species (Johnson et al., 2002; Welch et al., 2003).

Table 2
Speciation calculations using PHREEQC (Parkhurst and Appelo, 1999) for mixtures of solutions used in Experiments 3 and 4

Ph	mM		%Fe(II)			
	Fe(II)	HCO_3^-	$FeHCO_3^+$	$FeCO_3^{\circ}$	Fe^{2+}	$Fe(OH)^+$
4	0.01	0.02	45.0	<1	54.5	<1
4	0.01	0.015	37.5	<1	61.9	<1
4	0.01	0.01	27.9	<1	71.3	<1
4	0.01	0.005	15.8	<1	83.2	<1
7	0.004	0.01	31.5	2.7	64.8	<1
7	0.004	0.005	18.7	1.6	78.4	<1
7	0.004	0.001	4.3	<1	93.8	<1
7	0.004	0.0005	2.2	<1	96.1	<1

All calculations at 20 °C. The speciation of Fe(II) has been modeled using $FeCl_2$ as a proxy because $Fe(ClO_4)_2$ is not included in the PHREEQ database. At the conditions of our experiments, ClO_4^- is a less reactive ligand than Cl^-. The abundance of the mono-chloro complex $FeCl^+$ was always below 2%. Fe^{2+} is the hexaquo species $[Fe^{II}(H_2O)_6]^{2+}$.

3.1. Experiment 1—"*green rust*" precipitation

The pine-green precipitate that formed in Experiment 1 (Table 1) is most likely a mixture between a Fe(II)–Fe(III) phase, commonly referred to as "green rust" (e.g., Feitknecht and Keller, 1950; Hanson, 1989; Schwertmann and Fechter, 1994; Lewis, 1997; Génin et al., 1998; Cornell and Schwertmann, 2003) and siderite, and required the presence of traces of oxygen in the reaction vessel. During the course of the experiment, ~90% of the total aqueous Fe was converted to a precipitate (Fig. 2A). Assays of ferric and ferrous Fe contents of the aqueous Fe demonstrated that ~15% of the total iron in solution was ferric, which was significantly higher than in any other experiment (Table 3). Given the aqueous Fe^{II}/Fe(tot) ratios in Experiment 1 (Table 3), and the reported Fe^{II}/Fe^{III} ratios in "green rusts" of 0.8–3.6 (e.g., Cornell and Schwertmann, 2003), "green rust" could make up to ~70% of the solid precipitate, the remainder consisting most likely of siderite. At the conditions employed in Experiment 1, "green rust" is a likely product (Legrand et al., 2000; Cornell and Schwertmann, 2003). Following oxidation, $Fe(III)_{aq}$ was probably hydrolyzed rapidly under the conditions of Experiment 1 and precipitated as ferrihydrite, which then reacted with the remaining $Fe(II)_{aq}$ to produce "green rust". In addition, direct precipitation of "green rust" from $Fe(II)_{aq}$ is also possible. XRD spectra obtained on the green precipitate did not confirm the identity as "green rust", although clearly indicated that siderite was not produced in significant quantities. It is likely that exposure of the fine-grained, damp material to air, even for a short time (minutes), oxidized a significant proportion of the solid to fine grained ferrihydrite, which would not produce distinctive XRD spectra. However, SEM imaging revealed the presence of hexagonal platelets (Fig. 1D), which is a characteristic morphology of "green rust" (Legrand et al., 2000; Cornell and Schwertmann, 2003).

Because predicted (Polyakov and Mineev, 2000; Schauble et al., 2001) and measured (Johnson et al.,

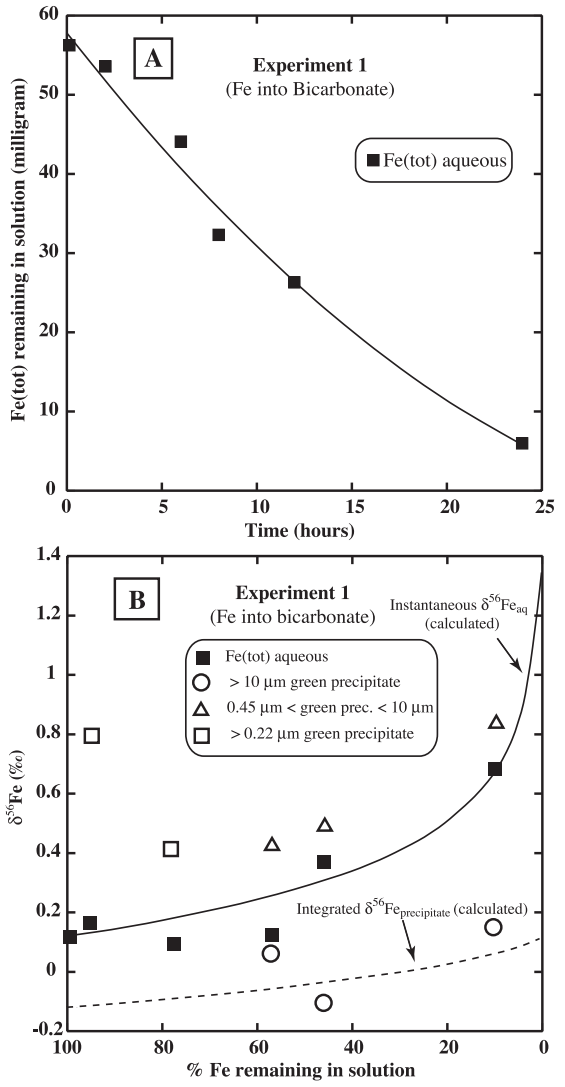

Fig. 2. (A) Plot of time versus Fe(tot) remaining in solution in Experiment 1. The perchlorate solution was rapidly (~10 s) introduced into the bicarbonate solution by means of a pressure head. About 90% of the introduced Fe was converted into a green precipitate (likely a mixture of "green rust" and siderite) by the end of the experiment. The solid line has been calculated using a first order integrated rate law $[\ln(1-F)=-K_1 t]$ with $K_1=-0.0669\ h^{-1}$. K_1 has been obtained by linear regression (intercept forced through zero) with a correlation coefficient (r^2) of 0.98. (B) Plot of $\delta^{56}Fe$ of $Fe(tot)_{aq}$ and different size fractions of the precipitate (most likely a mixture of "green rust" and siderite) versus the percentage of Fe remaining in solution for Experiment 1. Error bars are about the size of the symbols used. The instantaneous $\delta^{56}Fe_{aq}$ (solid line) has been calculated using a Rayleigh equation and $\alpha_{Precipitate\text{-}Fe(II)}=0.99976$, obtained by linear regression (not shown). The dashed line indicates the integrated average $\delta^{56}Fe$ of the green precipitate as calculated using a Rayleigh equation and $\alpha_{Precipitate\text{-}Fe(II)}=0.99976$.

2002; Welch et al., 2003) fractionation between ferric and ferrous Fe phases are generally large, it is expected that variations in the Fe^{II}/Fe^{III} ratios in "green rust" are likely to produce significant changes in Fe isotope fractionation between aqueous Fe and solid. In Experiment 1, the $\delta^{56}Fe$ values for the aqueous Fe are consistently higher than those of the large solid fraction (>10 μm) (Fig. 2B), but are lower than those of the finer-grained (0.45–10 μm) size fraction (Fig. 2B). These observations are markedly different than those of the siderite experiments (below), where the $\delta^{56}Fe$ of the fine-grained fraction initially track those of aqueous Fe, followed by a convergence with the large (>10 μm diameter) solid fraction. Because "green rust" is a mixed ferric–ferrous phase (e.g., Cornell and Schwertmann, 2003), it is possible that the fine-grained solid fraction has a different ferric/ferrous ratio than the larger fraction, which therefore could have a significantly different Fe

Table 3
Fe isotope data for Experiment 1

Sample name	Time (h)	$\delta^{56}Fe$	2 S.E.[a]	$\delta^{57}Fe$	2 S.E.	Fe(II)/Fe(tot)[b]
Fe aqueous						
2F-1365	0	0.12[c]	0.06	0.19	0.04	0.958
2F-1366	2	0.16[c]	0.05	0.19	0.04	0.858
2F-1368	6	0.09[c]	0.06	0.17	0.04	0.922
2F-1370	8.16	0.14[c]	0.03	0.28	0.04	0.762
2F-1373	11.5	0.37[c]	0.06	0.51	0.04	0.888
2F-1376	23.8	0.69[c]	0.06	1.07	0.04	0.881
Solid fraction >10 μm						
2F-1371	8.16	0.06	0.06	0.06	0.04	
2F-1374	11.5	−0.07	0.05	−0.07	0.03	
2F-1377[d]	23.8	0.13	0.07	0.25	0.03	
Solid fraction between 0.45 and 10 μm						
2F-1372	8.16	0.43	0.07	0.56	0.04	
2F-1375	11.5	0.49	0.07	0.75	0.05	
2F-1378	23.8	0.84	0.05	1.20	0.03	
Solid fraction >0.22 μm						
2F-1367	2	0.82	0.07	1.30	0.04	
2F-1369	6	0.41	0.06	0.62	0.04	

[a] 2 S.E. (standard error) calculated from in-run statistics.
[b] Determined using the *Ferrozine* method.
[c] Data used for regression of α.
[d] XRD spectra of the final precipitate (>10 μm size fraction) did not confirm the presence of siderite, "green rust" or any (hydrous) ferric oxides. The lack of any discernible spectra may be explained by the amorphous, fine-grained nature of the precipitate.

isotope fractionation. A fractionation factor of $10^3 \ln\alpha_{\text{Liquid-precipitate}} = \sim +0.25‰$ has been obtained by regression (not shown). Given that the >10-μm sized fraction makes up the largest part of a given sample, the calculated fractionation factor may be relevant between aqueous iron and the larger-sized precipitate, although the identity and the Fe(II)/Fe(III) ratio of the precipitate are not well constrained. These issues are deserving of further experimental study.

3.2. Experiment 2—rapid precipitation of siderite

Preliminary, extremely rapid synthesis of siderite (a few seconds), obtained through mixing sodium bicarbonate (0.01 mol/l) and ferrous perchlorate (0.005 mol/l), produced no discernable isotopic fractionation between aqueous Fe(II) (δ^{56}Fe=0.19‰) and precipitated siderite (δ^{56}Fe=0.15‰) within analytical uncertainty of our long-term reproducibility (±0.10‰, 2 S.D.). The reaction converted about 15% of the total initial aqueous Fe to siderite in 10 min. At the concentrations used, supersaturation produces instantaneous precipitation, which likely prevented isotopic fractionation between dissolved and solid Fe components. Similar results during extremely rapid precipitation have been observed, for example, for oxygen isotopes in calcite precipitation experiments (McCrea, 1950), as well as for iron isotopes in hematite precipitation experiments (Skulan et al., 2002).

Slower, although still rapid, precipitation of siderite (order of hours) occurred in Experiment 2, where precipitation was induced by pumping ferrous perchlorate solution into a sodium bicarbonate solution where the final Fe/carbonate ratio was 1:2 on a molar basis (Table 1). Except for the "instantaneous" experiment described above, initial precipitation rates were highest in this experiment, where near-complete precipitation of aqueous Fe(II) to siderite occurred within ~11 h (Fig. 3A). Siderite produced in this experiment (confirmed by XRD) consisted of spherical globules or aggregates of globules that had sizes varying from ~1 to ~10 μm (Fig. 1A, B and C). The initial anhedral surface of the siderite globules is replaced by a mosaic of euhedral, small aggregates on the surface of the globules after ~6 h (Fig. 1B and C). Similar carbonate globules have been reported in precipitation experiments by Golden et al. (2000), although they used mixed Ca–Mg–Fe–Mn solutions

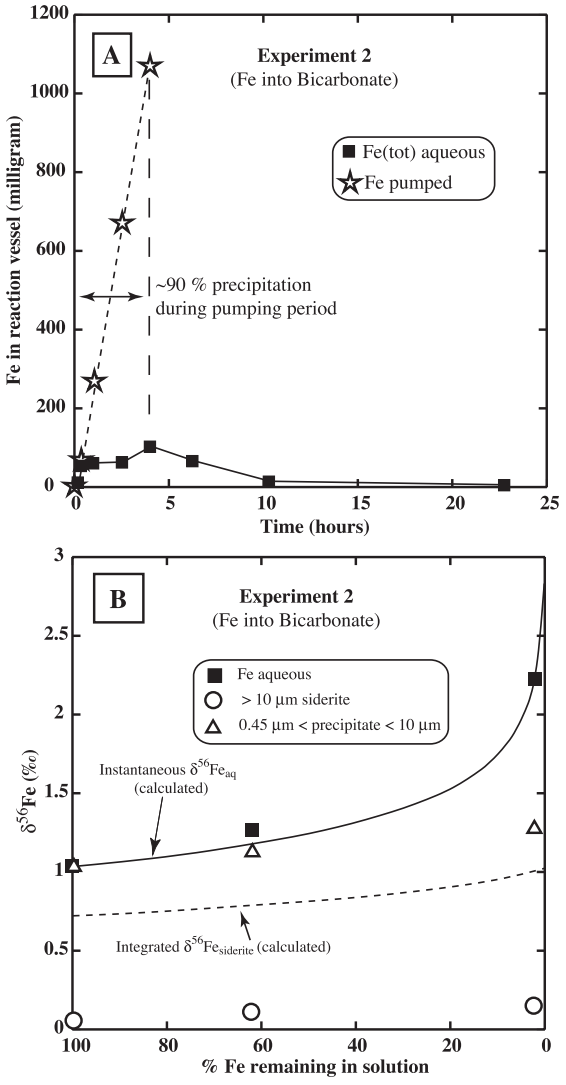

Fig. 3. (A) Plot of time versus Fe(tot) in the reaction vessel in Experiment 2. The dashed line indicates the amount of ferrous perchlorate solution pumped into the bicarbonate solution at a rate of 0.16 ml/min. About 90% of the introduced Fe precipitated as siderite during the pumping period, which lasted 4 h. After approximately 10 h, all available aqueous Fe has been consumed and precipitated as siderite. (B) Plot of δ^{56}Fe of Fe(tot)_{aq} and different size fractions of the solid versus the percentage of Fe remaining in solution in Experiment 2. Errors bars are about the size of the symbols used. Only data points after the active pumping stage (which stopped at time point 4 h) are shown. The instantaneous $\delta^{56}\text{Fe}_{aq}$ (solid line) has been calculated using a Rayleigh equation and $\alpha_{\text{Siderite-Fe(II)}}$=0.99969, obtained by linear regression (see Fig. 6). The dashed line indicates the integrated average isotope composition of the precipitate, calculated using a Rayleigh equation and $\alpha_{\text{Siderite-Fe(II)}}$=0.99969 (see text for an explanation).

and all but one set of their experiments were conducted at 150 °C. Rapid production of biogenic siderite over several days produced nearly identical morphologies as observed in Experiment 2 (Fig. 1A, B and C), whereas over timescales of weeks to months, rhombohedral morphologies were produced during biogenic magnetite and siderite production (Johnson et al., 2004). Because siderite in nature most commonly exists as rhombohedral forms, we assume that such morphologies more closely represent equilibrium conditions.

Iron isotope compositions for experimental run products were determined on different size fractions, including >10 and 0.45–10 μm, where it was anticipated that different size fractions may be dominated by different morphologies (Table 4). As expected during rapid precipitation in Experiment 2 (Fig. 3A and B, Table 4), initial isotopic differences between $Fe(II)_{aq}$ and the two siderite size fractions were small. However, after the active pumping stage, when ~90% of the Fe in the system resided in the precipitated solid, the minor proportions of $Fe(II)_{aq}$ in the system produced the largest isotopic changes in that component. The largest reservoir of Fe in the later part of the experiment lies in the siderite fraction that is greater than 10 μm in diameter, which, as required by mass balance, has a relatively constant δ^{56}Fe composition ~+0.10‰. The discrepancy between the δ^{56}Fe values for the >10-μm fraction and the integrated δ^{56}Fe of the solid (Fig. 3B, dashed line) reflects the

Table 4
Fe isotope data for Experiment 2

Sample name	Time (h)	δ^{56}Fe	2 S.E.[a]	δ^{57}Fe	2 S.E.	Fe(II)/Fe(tot)[b]
Fe aqueous						
3F-241	0.25	0.16	0.06	0.26	0.04	0.584
3F-243	1.00	0.22	0.07	0.31	0.04	0.527
3F-246	2.50	1.02	0.05	1.47	0.04	0.710
3F-249	4.00	1.04[c]	0.05	1.61	0.04	0.909
3F-252	6.25	1.25[c]	0.06	1.93	0.05	0.880
3F-255	10.25	2.20[c]	0.06	3.25	0.04	1.000
Siderite fraction >10 μm						
3F-244	1.00	0.15	0.06	0.22	0.04	1.000
3F-247[d]	2.50	0.10	0.06	0.12	0.03	0.969
3F-250	4.00	0.05	0.06	0.12	0.04	0.792
3F-253[d]	6.25	0.10	0.06	0.18	0.05	1.000
3F-256	10.25	0.14	0.06	0.09	0.06	1.000
Solid fraction between 0.45 and 10 μm						
3F-242	0.25	0.15	0.07	0.27	0.05	0.752
3F-245	1.00	0.67	0.06	1.02	0.03	0.730
3F-248	2.50	1.36	0.05	2.07	0.04	0.754
3F-251	4.00	1.01	0.05	1.53	0.04	0.841
3F-254	6.25	1.13	0.09	1.65	0.04	–
3F-257	10.25	1.27	0.07	1.81	0.04	0.784

Sample name	Dissolution time (min)	δ^{56}Fe	2 S.E.	δ^{57}Fe	2 S.E.	% Partial dissolution
Partial dissolution of siderite >10 μm						
3F-236 (leach)[e]	3	−0.02	0.07	0.06	0.06	20.1
3F-237 (leach)[f]	3	0.08	0.08	0.14	0.05	65.7

[a] 2 S.E. (standard error) calculated from in-run statistics.
[b] Determined using the *Ferrozine* method.
[c] Data used for regression of α.
[d] XRD analysis confirmed it as siderite.
[e] The siderite fraction >10 μm sampled at 6.25 h, partially dissolved in 0.1 M HCl for 3 min.
[f] Siderite fraction >10 μm sampled at 31 h, partially dissolved in 0.1 M HCl for 3 min.

fact that for the calculations, the isotope value of $Fe(II)_{aq}$ of time point 4 h was used as the initial value. In contrast, the smaller siderite fraction tracks the $\delta^{56}Fe$ of the $Fe(II)_{aq}$ component and attains a final $\delta^{56}Fe$ value of +1.27‰. Upon near complete conversion of $Fe(II)_{aq}$ to siderite after ~10 h, the isotopic difference between $Fe(II)_{aq}$ and the smaller solid fraction is +0.93‰ (Fig. 3B). Partial dissolutions of the >10-μm size siderite fraction from time points 6.25 and 31 h in 0.1 M HCl dissolved ~20% and 65% of the solid, respectively, but produced negligible isotopic variability relative to the bulk solid (Table 4), indicating that the larger-sized siderite fraction contains little isotopic variability.

3.3. Experiment 3 (method 1)—slow precipitation of siderite

The design of Experiment 3 was similar to that of Experiment 2, except that lower concentrations of reagents were used to decrease the rate of siderite precipitation, and the final Fe/carbonate ratio was equal on a molar basis and did not use excess carbonate ion as in Experiment 2 (Table 1). In contrast to Experiment 2, only negligible precipitation occurred during the introduction of the ferrous perchlorate solution (Fig. 4A), thus the measured $\delta^{56}Fe$ values for the >10-μm size siderite fraction agrees well with the calculated integrated $\delta^{56}Fe$ values of the solid (Fig. 4B, dashed line). Precipitation of siderite was allowed to proceed for 29 h, at which point ~60% conversion of $Fe(II)_{aq}$ to siderite occurred (Fig. 4A). XRD spectra obtained on the final precipitate (>10-μm fraction) confirmed it to be siderite.

The $\delta^{56}Fe$ of $Fe(II)_{aq}$ increases with time from +0.13‰ to a final value of +0.74‰ (Table 5, Fig. 4B). Both size fractions (>10 and 0.22–10 μm) of the solid phase undergo relatively large fluctuations in $\delta^{56}Fe$ values during the initial part of the experiment. In particular, the initial $\delta^{56}Fe$ value of the fine-grained solid fraction at time point 0.66 h is +1.27‰, which, relative to other experiments, appears anomalously high (Table 5). Because the small solid fraction early in the experiment comprises only a small component of the total Fe in the system, in addition to the slow precipitation rates, we suggest that the anomalously high $\delta^{56}Fe$ values of the early fine-grained fraction likely reflects an oxidized Fe solid that was produced

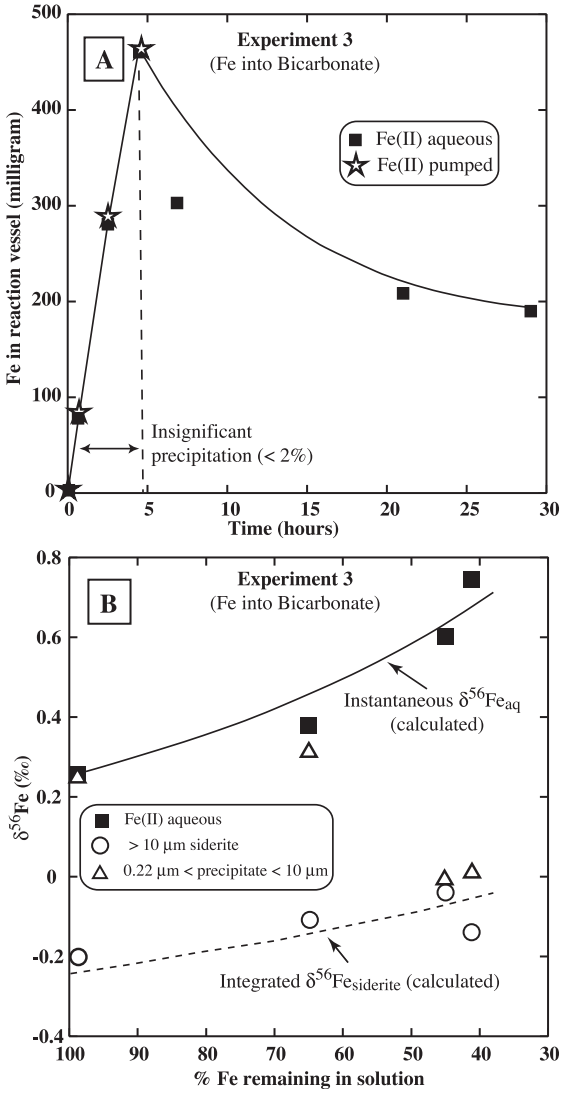

Fig. 4. (A) Plot of time versus Fe in the reaction vessel for Experiment 3. About 60% of the Fe reacted to siderite by the time the experiment was terminated. Only insignificant precipitation occurred during the pumping stage (<2%), which lasted for ~4 h. The curved segment of the solid line has been calculated using a second order integrated rate law $[F/(1-F)=K_2t]$ with $K_2=0.0646\ h^{-1}$. K_2 has been obtained by linear regression (intercept forced through 0) with a correlation coefficient (r^2) of 0.85. (B) Plot of $\delta^{56}Fe$ of $Fe(tot)_{aq}$ and the different size fractions of siderite versus the percentage of Fe(tot) remaining in solution for Experiment 3. Error bars are about the size of the symbols used. The instantaneous $\delta^{56}Fe_{aq}$ (solid line) has been calculated using a Rayleigh equation and an $\alpha_{Siderite\text{-}Fe(II)}=0.99951$ obtained by linear regression (see Fig. 6). The dashed line indicates the integrated average $\delta^{56}Fe$ of the siderite precipitate, calculated using a Rayleigh equation and $\alpha_{Siderite\text{-}Fe(II)}=0.99951$. As in the previous experiment, only $\delta^{56}Fe$ values after the active pumping stage have been used to calculate α by linear regression (Fig. 6).

Table 5
Fe isotope data for Experiment 3

Sample name	Time (h)	δ^{56}Fe	2 S.E.[a]	δ^{57}Fe	2 S.E.	Fe(II)/Fe(tot)[b]
Fe aqueous						
3F-1124	0.66	0.13	0.04	0.25	0.03	0.999
3F-1126	2.5	0.11	0.06	0.21	0.03	0.994
3F-1129	4.5	0.25[c]	0.05	0.38	0.03	0.957
3F-1132	6.8	0.38[c]	0.05	0.56	0.03	0.999
3F-1135	21	0.60[c]	0.05	0.93	0.03	0.994
3F-1138	29	0.74[c]	0.05	1.02	0.04	0.993
Siderite fraction >10 μm						
3F-1127	2.5	0.42	0.05	0.57	0.04	0.705
3F-1130	4.5	−0.20	0.06	−0.36	0.04	0.960
3F-1133	6.8	−0.11	0.05	−0.19	0.03	0.953
3F-1136	21	−0.04	0.05	−0.11	0.03	0.999
3F-1139[d]	29	−0.14	0.05	−0.21	0.03	0.997
Solid fraction between 0.22 and 10 μm						
3F-1125	0.66	1.27	0.05	1.81	0.04	–
3F-1128	2.5	0.20	0.04	0.2	0.03	0.466
3F-1131	4.5	0.25	0.04	0.23	0.03	–
3F-1134	6.8	0.31	0.05	0.45	0.03	0.595
3F-1137	21	−0.01	0.03	−0.09	0.03	0.966
3F-1140	29	0.01	0.07	0.04	0.04	0.907

Sample name	Dissolution time (min)	δ^{56}Fe	2 S.E.	δ^{57}Fe	2 S.E.	% Partial dissolution
Partial dissolution of siderite >10 μm[e]						
3F-1236 (leach)	5	−0.32	0.06	−0.42	0.02	3.7
3F-1237 (resid.)		−0.09	0.05	−0.15	0.03	
3F-1238 (leach)	10	−0.25	0.04	−0.41	0.03	4.9
3F-1239 (resid.)		−0.05	0.04	−0.12	0.03	

[a] 2 S.E. (standard error) calculated from in-run statistics.
[b] Determined by the *Ferrozine* method.
[c] Data used for regression of α.
[d] XRD spectra confirmed the solids to be siderite.
[e] Siderite fraction (>10 μm) sampled at 29 h.

early in the experiment by residual traces of O_2. Oxidation of $Fe(II)_{aq}$ would be expected to produce solids that have high δ^{56}Fe values (Bullen et al., 2001; Johnson et al., 2002; Welch et al., 2003). During later stages of the experiment, when the fraction of siderite is more substantial, any isotopic effect due to oxidation would be negligible. Another possibility is that a precurser phase of siderite was present early in the experiment, which, during aging, apparently approaches the isotopic compositions of the larger siderite fraction in the later stages of the experiment (Fig. 4B). Partial dissolutions of the final siderite (>10-μm fraction) in 0.1 M HCl for 5 and 10 min yielded δ^{56}Fe values that are ~0.15‰ lower than the bulk-δ^{56}Fe values of the siderite at 3.7% and 4.9% dissolution (Table 5), indicating small amounts of isotopic heterogeneity in the bulk siderite.

3.4. Experiment 4 (method 2)—slow precipitation of siderite

Experiment 4 involved identical overall proportions of reagents and pumping rates as Experiment 3, except that instead of pumping the ferrous perchlorate solution into the sodium bicarbonate solution, the sodium bicarbonate was pumped into the ferrous

perchlorate solution (Table 1). As in Experiment 3, about 60% of the initial $Fe(II)_{aq}$ was converted to siderite after ~48 h (Fig. 5A). XRD spectra confirmed that the precipitate >10 μm in size was siderite.

Iron isotope compositions of $Fe(II)_{aq}$ varied over the time of the experiment, where $\delta^{56}Fe$=+0.13‰ at the beginning of the experiment and increased to a final $\delta^{56}Fe$ value of +0.58‰ (Table 6). The >10-μm size siderite fraction had a relatively constant $\delta^{56}Fe$ value of ~−0.34% throughout the experimental run. An integrated average $\delta^{56}Fe$ composition of the total precipitate has been calculated (see Fig. 5B), but does not agree by mass balance calculations with the $\delta^{56}Fe$ values of the larger-sized siderite, because precipitation already occurred at the beginning of the experiment, and only time points after the pumping stage have been used to calculate the integrated $\delta^{56}Fe$ of the total solid (Fig. 5B). However, the integrated $\delta^{56}Fe$ values of the precipitate agree well with $\delta^{56}Fe$ values obtained from partial dissolutions (Table 6). The 0.22–10-μm size solid fraction had similar temporal trends in isotopic compositions as those observed in Experiment 3, where initially high $\delta^{56}Fe$ values decrease over the experimental run, and at the end of the experiment, are similar to those of the >10-μm fraction (Fig. 5B). In partial dissolutions of the final siderite (>10-μm size fraction) using 0.1 M HCl, 5.6% and 7.3% of the siderite was dissolved in 5- and 10-min treatments, respectively, and this treatment produced no distinguishable differences in $\delta^{56}Fe$ values (Table 6), indicating that little isotopic variability existed in the large siderite fraction.

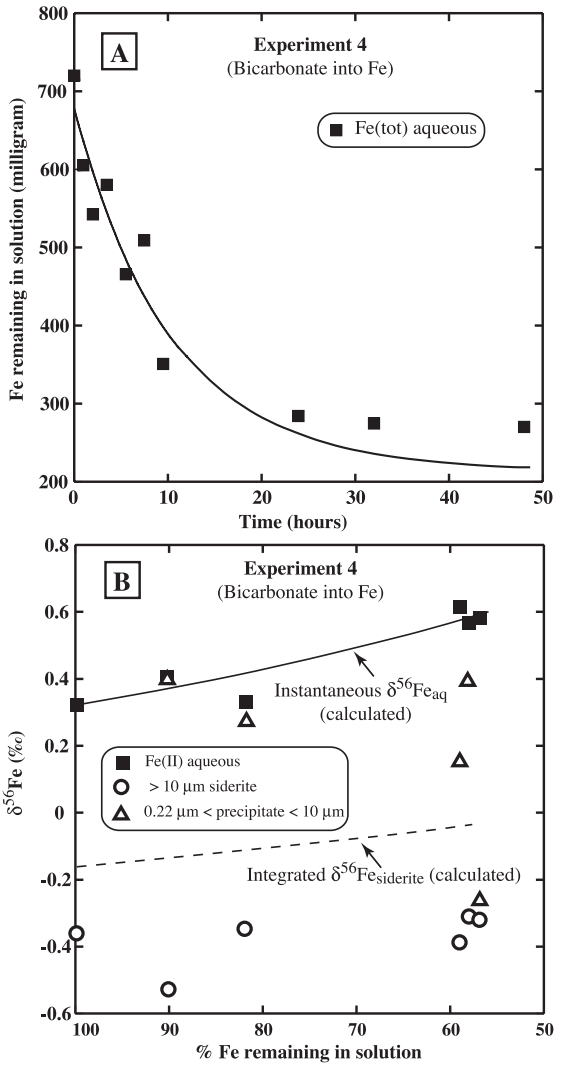

Fig. 5. (A) Plot of time versus Fe remaining in solution for Experiment 4. The bicarbonate solution was introduced into the perchlorate solution at a rate of 0.16 ml/min. Similar to Experiment 3, about 60% of the Fe was converted to siderite during the experiment. The solid line has been calculated using a second order integrated rate law ($F/(1-F)=K_2t$) with K_2=0.0692 h^{-1}. K_2 has been obtained by linear regression (intercept forced through 0) with a correlation coefficient (r^2) of 0.98, using data points up to 20 h. Later data points deviate from a second order rate equation and may reflect a different mechanism of precipitation. (B) Plot of $\delta^{56}Fe$ of $Fe(tot)_{aq}$ and the different size fractions of siderite versus the percentage of Fe remaining in solution in Experiment 4. Error bars are about the size of the symbols used. Only data points after the active pumping stage (which stopped at time point ~5 h) are shown. The instantaneous $\delta^{56}Fe_{aq}$ (solid line) has been calculated using a Rayleigh equation and an $\alpha_{Siderite\text{-}Fe(II)}$=0.99952, as obtained by linear regression. The dashed line indicates the integrated average $\delta^{56}Fe$ of the solid phase, calculated using a Rayleigh equation and $\alpha_{Siderite\text{-}Fe(II)}$=0.99952 (see text for an explanation). Similar to the previous experiments, only $\delta^{56}Fe$ values after the active pumping stage have been used to calculate α by linear regression (Fig. 6).

3.5. Estimation of equilibrium isotope fractionation between $Fe(II)_{aq}$ and siderite

The Fe isotope variations during precipitation that were observed in the three siderite experiments follow a Rayleigh-fractionation model, and our preferred fractionation factor between $Fe(II)_{aq}$ and siderite is $10^3\ln\alpha_{Fe(II)\text{–}Siderite}$=+0.48±0.22‰. Linear regression of Experiments 2, 3 and 4 were performed using

Table 6
Fe isotope data for Experiment 4

Sample name	Time (h)	δ^{56}Fe	2 S.E.[a]	δ^{57}Fe	2 S.E.	Fe(II)/Fe(tot)[b]
Fe aqueous						
3F-1201	0.0	0.13	0.05	0.23	0.04	0.974
3F-1202	1.0	0.18	0.05	0.31	0.03	0.989
3F-1204	2.0	0.15	0.05	0.24	0.04	0.970
3F-1206	3.5	0.26	0.06	0.43	0.03	0.999
3F-1209	5.5	0.32[c]	0.05	0.43	0.03	0.983
3F-1212	7.5	0.40[c]	0.07	0.57	0.03	0.974
3F-1215	9.5	0.33[c]	0.06	0.45	0.03	0.999
3F-1218	24.0	0.62[c]	0.05	0.87	0.03	0.966
3F-1221	32.0	0.57[c]	0.06	0.81	0.04	0.994
3F-1224	48.0	0.58[c]	0.05	0.84	0.03	0.975
Siderite fraction >10 μm						
3F-1207	3.5	−0.23	0.04	−0.28	0.03	0.826
3F-1210	5.5	−0.36	0.05	−0.59	0.03	0.959
3F-1213	7.5	−0.53	0.06	−0.75	0.04	0.950
3F-1216	9.5	−0.35	0.06	−0.55	0.04	0.976
3F-1219	24.0	−0.39	0.06	−0.63	0.03	0.920
3F-1222	32.0	−0.31	0.05	−0.44	0.03	0.942
3F-1225[d]	48.0	−0.32	0.07	−0.39	0.04	0.896
Solid fraction between 0.22 and 10 μm						
3F-1203	1.0	2.54	0.05	3.78	0.04	0.066
3F-1205	2.0	1.48	0.06	2.17	0.03	0.270
3F-1208	3.5	0.21	0.05	0.32	0.03	0.757
3F-1214	7.5	0.41	0.06	0.56	0.03	0.805
3F-1217	9.5	0.28	0.05	0.42	0.03	0.753
3F-1220	24.0	0.16	0.04	0.18	0.02	0.887
3F-1223	32.0	0.39	0.06	0.7	0.03	0.934
3F-1226	48.0	−0.25	0.05	−0.29	0.03	0.890

Sample name	Dissolution time (min)	δ^{56}Fe	2 S.E.	δ^{57}Fe	2 S.E.	% Partial dissolution
Partial dissolution of siderite >10 μm[e]						
3F-1240 (leach)	5	−0.21	0.06	−0.39	0.03	5.6
3F-1241 (resid.)		−0.20	0.05	−0.41	0.03	
3F-1242 (leach)	10	−0.30	0.05	−0.46	0.03	7.3
3F-1243 (resid.)		−0.23	0.05	−0.36	0.03	

[a] 2 S.E. (standard error) calculated from in-run statistics.
[b] Determined by the *Ferrozine* method.
[c] Data used for regression of α.
[d] XRD spectra confirmed it as siderite.
[e] Siderite fraction sampled at 48 h.

Isoplot (Ludwig, 2003), assuming no errors in the fraction of Fe remaining, and produced the following results (Fig. 6):

$$10^3 \ln\alpha_{\mathrm{Fe(II)-Siderite}} = +0.31 \pm 0.34‰ \text{(Experiment 2)}$$
$$10^3 \ln\alpha_{\mathrm{Fe(II)-Siderite}} = +0.49 \pm 0.14‰ \text{(Experiment 3)}$$
$$10^3 \ln\alpha_{\mathrm{Fe(II)-Siderite}} = +0.48 \pm 0.18‰ \text{(Experiment 4)}$$

Because aqueous Fe concentrations changed rapidly during the initial stage in the experiments as $Fe(II)_{aq}$ (or bicarbonate in Experiment 4) was pumped into the system, it is difficult to calculate a *F*-value with confidence during this phase of the experiment. For this reason, time points during the active pumping stage have been excluded from the regressions in Fig. 6.

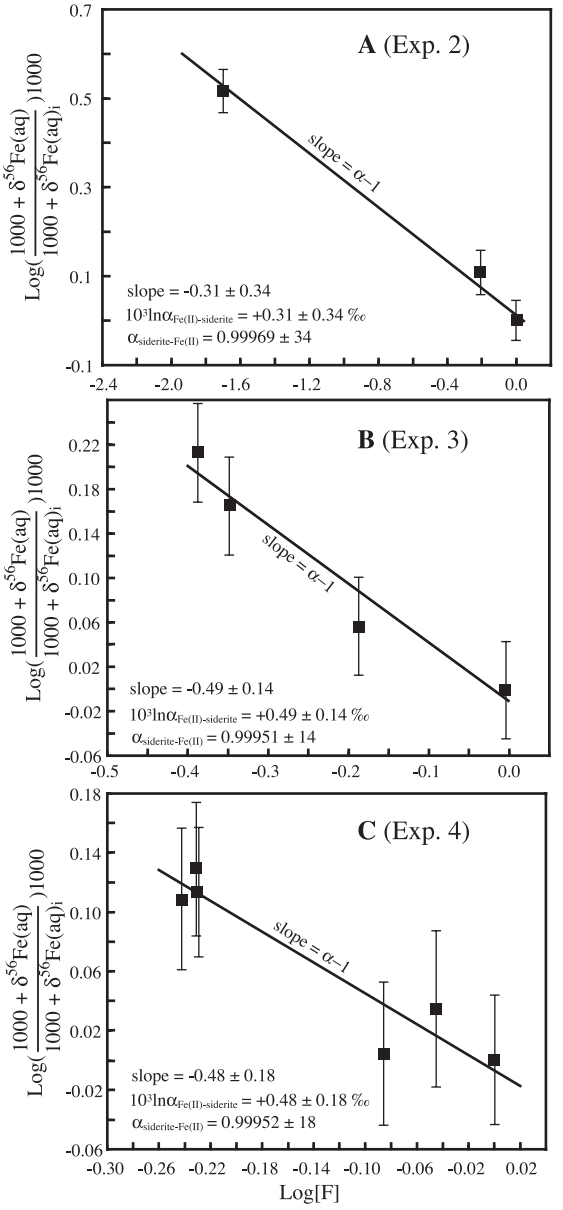

Fig. 6. Linear regressions of data from Experiments 2 (A), 3 (B) and 4 (C), using *Isoplot* (Ludwig, 2003). Errors for Log[F] have been assumed negligible. Only data obtained after the active pumping stage have been included in the regressions.

Rate constants were calculated for the different experiments to assess the relative rates of precipitation during an experimental run (Table 1, Fig. 7). Except for Experiment 1, which had the best correlation with a first order rate equation $[-d(1-F)/dt=K_1(1-F)]$, Experiments 2, 3 and 4 were more consistent with a second order rate equation $[-d(1-F)/dt=K_2(1-F)^2]$. Attempts to fit the data to other reaction orders resulted in lower r^2 values in the linear regressions. We note that our intent here is to constrain the relative rates of precipitation for the different experiments and not to use the rate equations to infer reaction mechanisms. The very high initial precipitation rates of Experiment 2 (Fig. 4), where ~90% precipitation occurred during the pumping stage, suggests that siderite produced in this experiment is more likely to record a kinetic isotopic fractionation as compared to Experiments 3 and 4, where insignificant amounts of precipitation occurred early in the experiments, and initial precipitation rates were significantly lower (Fig. 7). Moreover, because the maximum extent of precipitation was significantly less in Experiments 3 and 4, we interpret the fractionation factors from these experiments to more likely reflect equilibrium conditions.

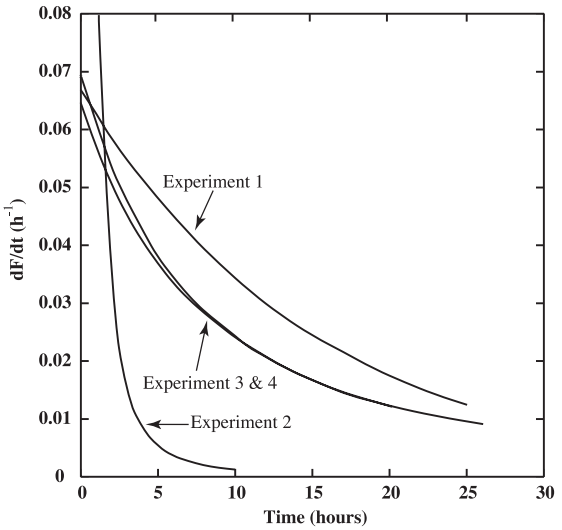

Fig. 7. Plot of change in rates (dF/dt) versus time for the precipitation experiments in this study. Except for Experiment 1, which yielded the best linear regression using a first order rate law (K_1=−0.0669, r^2=0.98), all other experiments were best fitted to a second order rate law (Experiment 2: K_2=6.9714 h^{-1}, r^2=0.83; Experiment 3: K_2=0.0646 h^{-1}, r^2=0.85; Experiment 4: K_2=0.0692 h^{-1}, r^2=0.98; in the linear regressions, intercepts were forced through zero). No reaction mechanisms are implied by the rate laws.

4. Discussion

Our results provide the first experimental constraints on the Fe isotope fractionation between

aqueous Fe(II) and siderite in abiotic systems at room temperatures. We first discuss the pathways involved in the synthesis experiments, which bear on the kinetic versus equilibrium issues that are always a concern in low-temperature synthesis experiments. Next, we compare our results to Fe isotope fractionations that are estimated from natural mineral assemblages. We also compare the experimentally determined fractionations from this study to those calculated using spectroscopic data (Polyakov, 1997; Polyakov and Mineev, 2000; Schauble et al., 2001). Finally, recent results from experiments that investigated Fe isotope fractionation produced during biogenic carbonate formation through dissimilatory reduction of hydrous ferric oxides are discussed in terms of possible differences in biologic and abiologic systems.

4.1. Kinetic versus equilibrium Fe isotope fractionation

A Rayleigh-type model best describes the Fe isotope variations in this study. If precipitation rates are sufficiently small, each increment of Fe precipitated as siderite may be in isotopic equilibrium with the instantaneous $Fe(II)_{aq}$. In this case, our inferred fractionation factors will reflect equilibrium. At the low temperatures at which our experiments where conducted, diffusional re-equilibration of Fe in the μm-range by solid-state diffusion is negligible; only dissolution–reprecipitation reactions may shift Fe isotope compositions of the solid.

The largest deviations from equilibrium are expected in the earlier time points of our experiments, where high degrees of supersaturation induced high precipitation rates, particularly for Experiment 2 (Fig. 7). Although it is possible that the early large positive δ^{56}Fe values for the smaller sized fractions may reflect kinetic Fe isotope fractionation between $Fe(II)_{aq}$ and a precurser phase of siderite (see Jimenez-Lopez and Romanek, 2004), we consider it more likely that oxidation of small amounts of $Fe(II)_{aq}$ to $Fe(III)_{aq}$ and subsequent precipitation to hydrous ferric oxide are the explanation for the higher δ^{56}Fe values of the fine-grained precipitates, given the large isotope fractionation of ~3‰ that occurs at room temperature between aqueous Fe(III) and Fe(II) (Johnson et al., 2002; Welch et al., 2003).

Based on partial dissolution experiments, particularly in Experiment 4, where both the dissolved and the residue portion are analytically indistinguishable (Table 6), siderite is relatively homogenous in terms of isotopic composition. Partial dissolution of the siderite precipitate is expected to preferentially dissolve the smaller particles and the outer surface of the larger siderite aggregates, components that are most likely to be in isotopic equilibrium with $Fe(II)_{aq}$. Using a $Fe(II)_{aq}$–siderite fractionation factor of +0.48‰ based on regression of Experiments 3 and 4, the δ^{56}Fe value of $Fe(II)_{aq}$ in equilibrium with the material dissolved during partial dissolution is ~+0.3‰, which is in good agreement with the actual δ^{56}Fe values of $Fe(II)_{aq}$ between time points 3.5 and 9.5 h (Table 6) where most of the precipitation has already occurred (~85%). Considering the lack of substantial isotopic zonation, in addition to the relatively slow initial precipitation rates of Experiments 3 and 4 (Fig. 7), it seems likely that isotopic equilibrium between $Fe(II)_{aq}$ and precipitated siderite was maintained in these experiments.

Oxygen isotope studies of the fractionations produced during precipitation of carbonates have some parallels to the current study. For example, it was recognized that the rate of precipitation has a major influence on the $^{18}O/^{16}O$ ratio of the precipitated carbonates (e.g., McCrea, 1950; O'Neil et al., 1969; Kim and O'Neil, 1997). Extremely rapid precipitation produced no O isotope difference between water and the carbonate, similar to the observation for Fe isotope fractionation, whereas slower precipitation rates produced significant isotope fractionation that may record either kinetic or equilibrium isotope partitioning. The specific reaction pathways for O and Fe isotope fractionation during carbonate precipitation experiments are, however, quite different. At our experimental conditions, siderite precipitation is most likely a surface controlled process, using calcite precipitation as an analog (e.g., Reddy and Nancollas, 1971), with the implication that the overall reaction rate is not determined by Fe transportation (diffusion) in the bulk aqueous solution.

A specific mechanistic model for siderite growth, which would allow evaluation of the kinetics of elementary reactions, does not yet exist. It is expected from studies of siderite ($FeCO_3$), rhodochrosite

($MnCO_3$) and calcite ($CaCO_3$) precipitation experiments (Greenberg and Tomson, 1992; Sternbeck, 1997; Nilsson and Sternbeck, 1999; Jimenez-Lopez and Romanek, 2004) that the rates involved in siderite growth are slower than those of calcite, but similar to those of rhodochrosite. The rate-limiting steps for siderite crystallization may be dehydration of adsorbed species such as $\equiv CO_3Fe^+ \cdot nH_2O$ on the surface (Pokrovsky and Schott, 2002), as well as adsorption onto dehydrated surface species such as $\equiv FeOH^o$ and CO_3H^o (Van Cappellen et al., 1993). Speciation calculations suggest that $FeHCO_3^+$ is one of the dominant species during the initial stages of precipitation in our experiments (Table 2), in addition to $[Fe^{II}(H_2O)_6]^{2+}$. $FeHCO_3^+$ may therefore be involved in surface complexation reactions such as $\equiv CO_3H^o + Fe^{2+} \Leftrightarrow \equiv CO_3Fe^+ + H^+$, $\equiv FeHCO_3^o \Leftrightarrow \equiv FeOH^o + CO_2$ and $\equiv FeCO_3^- + FeCO_3^o(aq) \Leftrightarrow \equiv FeCO_3^- + 6\ H_2O$ (Van Cappellen et al., 1993; Sternbeck, 1997). These elementary reactions may change during the course of an experiment as P_{CO_2}, pH and the proportion of Fe species evolve (Table 2).

It is possible that Fe isotope fractionation may occur between Fe-bearing complexes that were common in our experiments, including $[Fe^{II}(H_2O)_6]^{2+}$, $[Fe^{II}HCO_3(H_2O)_5]^+$ and $[Fe^{II}CO_3(H_2O)_6]^o$. The carbonate and bicarbonate species are most common early in our experiments (Table 2), and Fe isotope fractionation between these species and the initial precipitates may explain some of the unusual isotopic fractionations we observe between aqueous Fe and the initial precipitates. However, $[Fe^{II}(H_2O)_6]^{2+}$ is the dominant aqueous Fe species at the end of the experiments, and to the degree that our preferred fractionation factors are derived through regression of the later data points (Fig. 6), we conclude that these fractionations largely reflect the $[Fe^{II}(H_2O)_6]^{2+}$–$FeCO_3$ fractionation factor.

4.2. Comparison to other $Fe(II)_{aq}$–Fe carbonate fractionation factors

The experimental results from this study can be compared to calculated equilibrium fractionation factors based on spectroscopic data, as well as those estimated from natural assemblages. Combining calculated β factors from Polyakov and Mineev (2000) and Schauble et al. (2001) for the $Fe(II)_{aq}$–siderite system at 20 °C yields $\Delta^{56}Fe_{Fe(II)aq-Siderite} = +2.11‰$ (Fig. 8), after converting the $\beta_{57/54}$ of Polyakov and Mineev (2000) to $\beta_{56/54}$ values. The combined uncertainty in $\beta_{56/54}$ values for $[Fe^{II}(H_2O)_6]^{2+}$ and $FeCO_3$ is ~1.4‰ at room temperature (Schauble et al., 2001), which places the lower end of the predicted fractionation within that measured in the current study. Johnson et al. (2003) estimated the Fe isotope fractionation factors for siderite, magnetite, ankerite and hematite in Banded Iron Formations, which, in combination with the $\beta_{56/54}$ factor of Schauble et al. (2001) for $[Fe^{II}(H_2O)_6]^{2+}$, allows a range of fluid mineral fractionation factors to be calculated. Using this approach, Johnson et al. (2003) estimated the $[Fe^{II}(H_2O)_6]^{2+}$–$FeCO_3$ fractionation to lie in the range of −1.7‰ to +0.3‰ at 25 °C (Fig. 8). This range of values is ~1.8‰ to 3.8‰ lower than the theoretical prediction of +2.11‰, although the higher end overlaps our experimental determination of +0.48±0.22‰ (Fig. 8). The discrepancy of fractionation factors between our experiments and theoretical prediction may lie in inaccuracy of vibrational frequencies and simplifying assumptions used to model vibrational frequencies (e.g., Schauble, 2004).

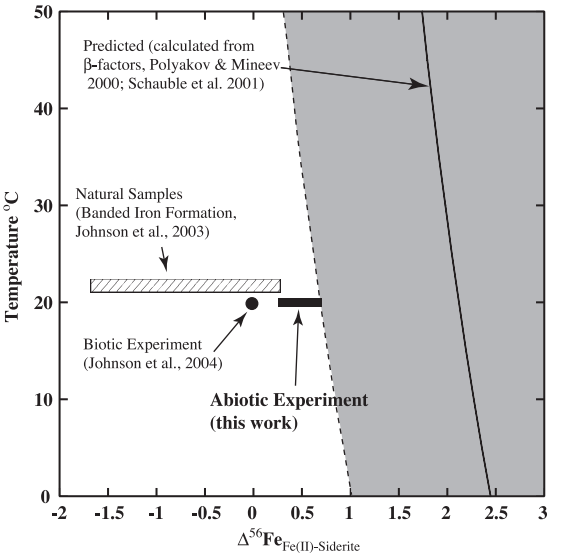

Fig. 8. Comparison of iron isotope fractionation between $Fe(II)_{aq}$ and siderite obtained by abiotic synthesis experiments (this work), biotic experiments (Johnson et al., 2004), natural siderite samples from BIFs (Johnson et al., 2003) and by prediction from spectroscopic data (Polyakov and Mineev, 2000; Schauble et al., 2001). Gray shaded area indicates error envelope for the predicted fractionation.

Recent studies involving dissimilatory Fe(III) reduction by bacteria (Beard et al., 1999, 2003a; Johnson et al., 2004) have shown that processing of iron by bacteria may or may not produce a measurable isotopic fractionation, depending on the mineral precipitated. Most pertinent to the current study is one of the experiments in Johnson et al. (2004), where dissimilatory Fe(III) reduction by *Shewanella putrefaciens* in a bicarbonate-buffered medium produced siderite where the estimated equilibrium $Fe(II)_{aq}$–siderite fractionation was ~0.0‰ at room temperature (22 °C). In contrast, addition of small amounts of Ca to the growth media resulted in precipitation of a Ca-substituted siderite ($\sim Ca_{0.15}Fe_{0.85}CO_3$) where the apparent equilibrium fractionation was ~+0.9‰ between $Fe(II)_{aq}$ and the Ca-bearing Fe carbonate. The change in Fe isotope fractionation upon Ca substitution in Fe–carbonates has been predicted from the calculated fractionation factor of Polyakov and Mineev (2000) and Schauble et al. (2001), and has been observed in natural samples (Johnson et al., 2003). Although determination of Fe isotope fractionation factors using various cation substitutions in siderite have not been made yet in abiologic systems, we would expect that Ca substitution will result in higher $Fe(II)_{aq}$–Fe carbonate fractionations then in the $Fe(II)_{aq}$–siderite system.

4.3. Application

Siderite from sedimentary rocks of mid-Archean to Cretaceous age generally have negative δ^{56}Fe values, but range from δ^{56}Fe=+0.5‰ to −1.5‰ (Johnson et al., 2003; Matthews et al., 2004; Yamaguchi et al., 2004). In many cases, siderite appears to have been directly precipitated from seawater or through early diagenetic reactions in marine basins, where, for example, $Fe(II)_{aq}$ and dissolved carbon react with hematite to form siderite and magnetite (e.g., Klein and Beukes, 1989; Beukes et al., 1990; Kaufman, 1996; Sumner, 1997). In Archean rocks, the likely source of large quantities of $Fe(II)_{aq}$ was Mid-Ocean Ridge (MOR) hydrothermal fluids (e.g., Klein and Beukes, 1989; Beukes et al., 1990). Iron isotope compositions of modern MOR hydrothermal fluids define a range of δ^{56}Fe from −0.69‰ to −0.21‰, with an average of −0.39±0.13‰ (Sharma et al., 2001; Beard et al., 2003b). If we assume that similar δ^{56}Fe values were characteristic Archean MOR hydrothermal fluids, as measured in modern MOR hydrothermal fluids, we would predict that δ^{56}Fe values for precipitated siderite should lie in the range of −1.18‰ to −0.69‰, using our experimentally derived fractionation factor of $10^3\ln\alpha_{Fe(II)-Siderite}$=+0.48±0.22‰ at 20 °C. The range of predicted δ^{56}Fe values for siderite agrees well with the δ^{56}Fe values measured for many siderite samples from Archean and Proterozoic Banded iron Formations (Johnson et al., 2003; Yamaguchi et al., 2004), suggesting that those Fe isotope compositions indicate precipitation from $Fe(II)_{aq}$ that was dominated by MOR sources, assuming that the δ^{56}Fe values of $Fe(II)_{aq}$ derived from MOR sources was the same as that measured today.

The $Fe(II)_{aq}$–$FeCO_3$ fractionation factor determined in this study, however, does not provide a ready explanation for siderite that has positive or near-zero δ^{56}Fe values, as are found in some banded iron formations and shales of Archean and Proterozoic age (Johnson et al., 2003; Yamaguchi et al., 2004). One explanation is that the δ^{56}Fe values of $Fe(II)_{aq}$ in the oceans was distinct from that measured today. A second possibility is that siderite that has high δ^{56}Fe values reflects different formation pathways then siderite which has low δ^{56}Fe values, accompanied by $Fe(II)_{aq}$ that had distinct Fe isotope compositions. Another factor influencing δ^{56}Fe values of siderite could be diagenetic or post-diagenetic mobilization of iron (e.g., Matthews et al., 2004). Finally, it is also possible that the variations in divalent cation contents of natural siderites, which commonly contain significant substitutions of Ca, Mg and Mn (e.g., Klein and Beukes, 1989), may exert a significant control on the $Fe(II)_{aq}$–carbonate isotope fractionation factors.

5. Conclusions

The Fe isotope fractionation between aqueous Fe(II) and siderite has been estimated at room temperature (~20 °C) using synthesis experiments, yielding $10^3\ln\alpha_{Fe(II)-Siderite}$=+0.48±0.22‰. Although true equilibrium cannot be demonstrated in these synthesis experiments, it is expected at the relatively slow precipitation rates observed in two experiments, kinetic effects were relatively minor, and isotope equilibrium was closely approached. In comparison to the $Fe(II)_{aq}$–siderite fractionations predicted from

spectroscopic data (Polyakov and Mineev, 2000; Schauble et al., 2001), our experimentally determined fractionation factor is ~1.5‰ lower at 20 °C, but lies at the margin of the uncertainty envelope estimated for the predicted fractionations. $Fe(II)_{aq}$–siderite fractionations inferred from natural assemblages range from −1.7‰ to +0.3‰ (Johnson et al., 2003), and the fractionation factor determined here lies on the high end of this range. Recent experiments involving dissimilatory Fe(III) reduction by bacteria with subsequent precipitation of siderite produced a measured $Fe(II)_{aq}$–siderite fractionation of ~0.0‰, which has been interpreted to reflect equilibrium conditions (Johnson et al., 2004). It is not yet clear if $Fe(II)_{aq}$–siderite fractionations can be uniquely related to biologic or abiologic systems. The $Fe(II)_{aq}$–$FeCO_3$ fractionation determined in this study well explains the moderately negative δ^{56}Fe values measured in many siderites in Archean and Proterozoic sedimentary rocks, assuming the major $Fe(II)_{aq}$ sources were Mid-Ocean Ridge hydrothermal fluids that had Fe isotope compositions that were similar to those measured today. Siderite that has near-zero or positive δ^{56}Fe values, however, are difficult to explain if they formed from low-δ^{56}Fe $Fe(II)_{aq}$, and may indicate distinct formation pathways, precipitation from distinct fluids, diagenetic or post-diagenetic alteration or the effects of cation substitution.

Acknowledgements

We would like to thank Sue Welch for assistance with SEM work and for help in processing samples. Reviews by A. Matthews and E. Mullane substantially improved the manuscript, and are greatly appreciated. This research was funded by the National Science Foundation through grant EAR-0106614 to CMJ and BLB. **[LW]**

References

Abdelmoula, M., Refait, P., Drissi, S.H., Mihé, J.P., Génin, J.-M.R., 1996. Conversion electron Mössbauer spectroscopy and X-ray diffraction studies of the formation of carbonate-containing green rust one by corrosion of metallic iron in $NaHCO_3$ and ($NaHCO_3$+NaCl) solutions. Corros. Sci. 38, 623–633.

Anbar, A.D., Roe, J.E., Barling, J., Nealson, K.H., 2000. Nonbiological fractionation of iron isotopes. Science 288, 126–128.

Baes, C.F., Mesmer, R.E., 1976. The Hydrolysis of Cations. Wiley and Sons, New York. 489 pp.

Bao, H., Koch, P.L., 1999. Oxygen isotope fractionation in ferric oxide–water systems: low temperature synthesis. Geochim. Cosmochim. Acta 63, 599–613.

Beard, B.L., Johnson, C.M., 1999. High precision iron isotope measurements of terrestrial and lunar materials. Geochim. Cosmochim. Acta 63, 1653–1660.

Beard, B.L., Johnson, C.M., 2004. Fe isotope variations in the modern and ancient Earth and other planetary bodies. In: Johnson, C.M., Beard, B.L., Albarède, F. (Eds.), Geochemistry of Non-Traditional Stable Isotopes, Reviews in Mineralogy and Geochemistry, vol. 55. Mineralogical Society of America and Geochemical Society, Washington, D. C., pp. 319–357.

Beard, B.L., Johnson, C.M., Cox, L., Sun, H., Nealson, K.H., Aguillar, C., 1999. Iron isotope biosignatures. Science 285, 1889–1892.

Beard, B.L., Johnson, C.M., Skulan, J.L., Nealson, K.H., Cox, L., Sun, H., 2003a. Application of Fe isotopes to tracing the geochemical and biological cycling of Fe. Chem. Geol. 195, 87–117.

Beard, B.L., Johnson, C.M., Von Damm, K.L., Poulson, R.L., 2003b. Iron isotope constraints on Fe cycling and mass balance in oxygenated Earth oceans. Geology 31, 629–632.

Beukes, N.J., Klein, C., Kaufman, A.J., Hayes, J.M., 1990. Carbonate petrography, kerogen distribution, and carbon and oxygen isotope variations in an early Proterozoic transition from limestone to iron-formation deposition, Transvaal Supergroup, South Africa. Econ. Geol. 85, 663–690.

Brantley, S.L., Liermann, L., Bullen, T.D., 2001. Fractionation of Fe isotopes by soil microbes and organic acids. Geology 29, 535–538.

Bullen, T.D., White, A.F., Childs, C.W., Vivit, D.V., Schulz, M.S., 2001. Demonstration of significant abiotic iron isotope fractionation in nature. Geology 29, 699–702.

Carothers, W.W., Adami, L.H., Rosenbauer, R.J., 1988. Experimental oxygen isotope fractionation between siderite–water and phosphoric acid liberated CO_2–siderite. Geochim. Cosmochim. Acta 52, 2445–2450.

Chacko, T., Cole, D.R., Horita, J., 2001. Equilibrium oxygen, hydrogen and carbon isotope fractionation factors applicable to geologic systems. In: Valley, J.W., Cole, D.R. (Eds.), Stable Isotope Geochemistry, Reviews in Mineralogy and Geochemistry, vol. 43. Mineralogical Society of America and Geochemical Society, Washington, D. C., pp. 1–81.

Cornell, R.M., Schwertmann, U., 2003. The Iron Oxides. Wiley-VCH, Weinheim. 664 pp.

Croal, L.R., Johnson, C.M., Beard, B.L., Newman, D.K., 2004. Iron isotope fractionation by Fe(II)-oxidizing photoautotrophic bacteria. Geochim. Cosmochim. Acta 68, 1227–1242.

Curtis, C.D., Coleman, M.L., Love, L.G., 1986. Pore water evolution during sediment burial from isotopic and mineral chemistry of calcite, dolomite and siderite concretions. Geochim. Cosmochim. Acta 50, 2321–2334.

Dawson, M., Lyle, S., 1990. Spectrophotometric determination of iron and cobalt with ferrozine and dithiozone. Talanta 37, 1189–1192.

Feitknecht, W., Keller, G., 1950. Über die dunkelgrünen Hydroxyverbindungen des Eisens. Z. Anorg. Allg. Chem. 262, 61–68.

Fredrickson, J.K., Zachara, J.M., Kennedy, D.W., Dong, H., Onstott, T.C., Hinman, N.W., Li, S., 1998. Biogenic iron mineralization accompanying the dissimilatory reduction of hydrous ferric oxide by a groundwater bacterium. Geochim. Cosmochim. Acta 62, 3239–3257.

Génin, J.-M.R., Bourrié, G., Trolard, F., Abdelmoula, M., Jaffrezic, A., Refait, P., Maitre, V., Humbert, B., Herbillon, A., 1998. Thermodynamic equilibria in aqueous suspensions of synthetic and natural Fe(II)–Fe(III) green rusts: occurrences of the mineral in hydromorphic soils. Environ. Sci. Technol. 32, 1058–1068.

Golden, D.C., Ming, D.W., Schwandt, C.S., Morris, R.V., Yang, S.V., Lofgren, G.E., 2000. An experimental study on kinetically-driven precipitation of calcium–magnesium–iron carbonates from solution: implications for the low-temperature formation of carbonates in martian meteorite Allan Hills 84001. Meteorit. Planet. Sci. 35, 457–465.

Greenberg, J., Tomson, M., 1992. Precipitation and dissolution kinetics and equilibria of aqueous ferrous carbonate vs. temperature. Appl. Geochem. 7, 185–190.

Hanson, H.C.B., 1989. Composition, stabilization, and light adsorption of Fe(II)Fe(III) hydroxy-carbonate ("green rust"). Clay Miner. 24, 663–669.

Hendry, J.P., 2002. Geochemical trends and paleohydrological significance of shallow burial calcite and ankerite cements in middle Jurassic strata on the East Midlands Shelf (onshore UK). Sediment. Geol. 151, 149–176.

Jimenez-Lopez, C., Romanek, C.S., 2004. Precipitation kinetics and carbon isotope partitioning of inorganic siderite at 25 °C and 1 atm. Geochim. Cosmochim. Acta 68, 557–571.

Johansson, G., Yokohama, H., 1990. Inner- and outer-sphere complex formation in aqueous erbium halide and perchlorate solutions. An X-ray diffraction study using isostructural substitution. Inorg. Chem. 29, 2460–2466.

Johnson, C.M., Skulan, J.L., Beard, B.L., Sun, H., Nealson, K.H., Braterman, P.S., 2002. Isotopic fractionation between Fe(III) and Fe(II) in aqueous solutions. Earth Planet. Sci. Lett. 195, 141–153.

Johnson, C.M., Beard, B.L., Beukes, N.J., Klein, C., O'Leary, J.M., 2003. Ancient geochemical cycling in the Earth as inferred from Fe isotope studies of banded iron formations from the Transvaal Craton. Contrib. Mineral. Petrol. 144, 523–547.

Johnson, C.M., Roden, E.E., Welch, S.A., Beard, B.L., 2004. Experimental constraints on Fe isotope fractionation during magnetite and Fe carbonate formation coupled to dissimilatory hydrous ferric oxide reduction. Geochim. Cosmochim. Acta (in press).

Kaufman, A.J., 1996. Geochemical and mineralogic effects of contact metamorphism on banded iron-formation: an example from the Transvaal Basin South Africa. Precambrian Res. 79, 171–194.

Kim, S.-T., O'Neil, 1997. Equilibrium and nonequilibrium oxygen isotope effects in synthetic carbonates. Geochim. Cosmochim. Acta 61, 3461–3475.

Klein, C., Beukes, N.J., 1989. Geochemistry and sedimentology of a facies transition from limestone to iron-formation deposition in the early Proterozoic Transvaal Supergroup, South Africa. Econ. Geol. 84, 1733–1774.

Klein, C., Beukes, N.J., 1992. Proterozoic iron-formations. In: Condie, K.C. (Ed.), Proterozoic Crustal Evolution. Elsevier, Amsterdam, pp. 383–418.

Legrand, L., Savoye, S., Chausse, A., Messina, R., 2000. Study of oxidation products formed on iron in solutions containing bicarbonate/carbonate. Electrochim. Acta 46, 111–117.

Lewis, D.G., 1997. Factors influencing the stability and properties of green rusts. In: Auerswald, K., Stanjek, H., Bigham, J.M. (Eds.), Advances in Geoecology, vol. 30. Catena, Reiskirchen, pp. 345–372.

Ludwig, K.R. 2003. User's manual for Isoplot 3.00, a geochronological toolkit for Microsoft *Excel*. Berkeley Geochronology Center Spec. Publ. No. 4, 74 pp.

Matthews, A., Zhu, X.-K., O'Nions, R.K., 2001. Kinetic iron stable isotope fractionation between iron (-II) and (-III) complexes in solution. Earth Planet. Sci. Lett. 192, 81–92.

Matthews, A., Morgans-Bell, H.S., Emmanuel, S., Jenkyns, H.C., Erel, Y., Halicz, L., 2004. Controls of iron-isotope fractionation in organic-rich sediments (Kimmeridge Clay, Upper Jurassic, southern England). Geochim. Cosmochim. Acta 68, 3107–3123.

McCrea, J.M., 1950. On the isotope chemistry of carbonates and the paleotemperature scale. J. Chem. Phys. 18, 849–857.

Misawa, T., Hashimoto, K., Shimodaira, S., 1973. Formation of Fe(II)1–Fe(III)1 intermediate green complex on oxidation of ferrous iron in neutral and slightly alkaline sulphate solutions. J. Inorg. Nucl. Chem. 35, 4167–4174.

Mozley, P.S., Carothers, W.W., 1992. Elemental and isotopic compositions of siderite in the Kuparuk formation, Alaska: effect of microbial activity and water/sediment interaction on early pore-water chemistry. J. Sediment. Petrol. 62, 681–692.

Nilsson, Ö., Sternbeck, J., 1999. A mechanistic model for calcite crystal growth using surface speciation. Geochim. Cosmochim. Acta 63, 217–225.

O'Neil, J.R., 1986. Theoretical and experimental aspects of isotopic fractionation. In: Valley, J.W., Taylor, H.P., O'Neil, J.R. (Eds.), Stable Isotopes in High Temperature Processes, Reviews in Mineralogy vol. 16. Mineralogical Society of America, Washington, D. C., pp. 1–40.

O'Neil, J.R., Clayton, R.N., Mayeda, T., 1969. Oxygen isotope fractionation in divalent metal carbonates. J. Chem. Phys. 51, 5547–5558.

Parkhurst, D.L., Appelo, C.A.J., 1999. User's guide to PHREEQC (version 2)—a computer program for speciation, batch-reaction, one-dimensional transport, and inverse geochemical calculations. Water-Resour. Invest. 99–4259, 287.

Parmar, N., Gorby, Y.A., Beveridge, T.J., Ferris, F.G., 2002. Formation of green rust and immobilization of nickel in response to bacterial reduction of hydrous ferric oxide. Geomicrobiol. J. 18, 375–385.

Pokrovsky, O.S., Schott, J., 2002. Surface chemistry and dissolution kinetics of divalent metal carbonates. Environ. Sci. Technol. (36), 426–432.

Polyakov, V.B., 1997. Equilibrium fractionation of the iron isotopes: estimation from Mössbauer spectroscopy data. Geochim. Cosmochim. Acta 61, 4213–4217.

Polyakov, V.B., Mineev, S.D., 2000. The use of Mössbauer spectroscopy in stable isotope geochemistry. Geochim. Cosmochim. Acta 64, 849–865.

Postma, D., 1982. Pyrite and siderite formation in brackish and freshwater swamp sediments. Am. J. Sci. 282, 1151–1183.

Pye, K., Dickson, J.A.D., Schiavon, N., Coleman, M.L., Cox, M., 1990. Formation of siderite–Mg–calcite–iron sulphide concretions in intertidal marsh and sandflat sediments, north Norfolk, England. Sedimentology 37, 325–343.

Raiswell, R., Fisher, Q.J., 2000. Mudrock-hosted carbonate concretions: a review of growth mechanisms and their influence on chemical and isotopic composition. J. Geol. Soc. 157, 239–251.

Reddy, M.M., Nancollas, G.H., 1971. The crystallization of calcium carbonate: I. Isotopic exchange and kinetics. J. Colloid Interface Sci. 36, 166–172.

Roe, J.E., Anbar, A.D., Barling, J., 2003. Nonbiological fractionation of Fe isotopes: evidence of an equilibrium isotope effect. Chem. Geol. 195, 69–85.

Schauble, E.A., 2004. Applying stable isotope fractionation theory to new systems. In: Johnson, C.M., Beard, B.L., Albarède, F. (Eds.), Geochemistry of Non-Traditional Stable Isotopes, Reviews in Mineralogy and Geochemistry vol. 55. Mineralogical Society of America and Geochemical Society, Washington, D. C., pp. 65–111.

Schauble, E.A., Rossman, G.R., Taylor, H.P., 2001. Theoretical estimates of equilibrium Fe-isotope fractionations from vibrational spectroscopy. Geochim. Cosmochim. Acta 65, 2487–2497.

Schwertmann, U., Fechter, H., 1994. The formation of green rust and its transformation to lepidocrocite. Clay Miner. 29, 87–92.

Schwertmann, U., Thalmann, H., 1976. The influence of [Fe(II)], [Si], and pH on the formation of lepidocrocite and ferryhydrate during oxidation of aqueous $FeCl_2$ solutions. Clay Miner. 11, 189–200.

Sharma, M., Polizzotto, M., Anbar, A.D., 2001. Iron isotopes in hot springs along the Juan de Fuca Ridge. Earth Planet. Sci. Lett. 194, 39–51.

Skulan, J.L., Beard, B.L., Johnson, C.M., 2002. Kinetic and equilibrium Fe isotope fractionation between aqueous Fe(III) and hematite. Geochim. Cosmochim. Acta 66, 2995–3015.

Stampfl, P.P., 1969. Ein basisches Eisen-II-III-Karbonat in Rost. Corros. Sci. 9, 14–22.

Sternbeck, J., 1997. Kinetics of rhodochrosite crystal growth at 25 °C: the role of surface speciation. Geochim. Cosmochim. Acta, 785–793.

Sumner, D.Y., 1997. Carbonate precipitation and oxygen stratification in late Archean seawater as deduced from facies and stratigraphy of the Gamohaan and Frisco Formations, Transvaal Supergroup, South Africa. Am. J. Sci. 297, 455–487.

Trolard, F., Génin, J.-M.R., Abdelmoula, M., Bourrié, G., Humbert, B., Herbillon, A., 1997. Identification of a green rust mineral in a reductomorphic soil by Mössbauer and Raman spectroscopies. Geochim. Cosmochim. Acta 61, 1107–1111.

Uysal, I.T., Golding, S.D., Glikson, M., 2000. Petrographic and isotope constraints on the origin of authigenic carbonate minerals and the associated fluid evolution in late Permian coal measures, Bowen Basin, (Queensland), Australia. Sediment. Geol. 136, 189–206.

Van Cappellen, P., Charlet, L., Stumm, W., Wersin, P., 1993. A surface complexation model of the carbonate mineral-aqueous solution interface. Geochim. Cosmochim. Acta 57, 3505–3518.

Welch, S.A., Beard, B.L., Johnson, C.M., Braterman, P.S., 2003. Kinetic and equilibrium Fe isotope fractionation between aqueous Fe(II) and Fe(III). Geochim. Cosmochim. Acta 67, 4231–4250.

Yamaguchi, K.E., Johnson, C.M., Beard, B.L., Ohmoto, H., 2004. Biogeochemical cycling of iron in the Archean–Paleoproterozoic Earth: constraints from iron isotope variations in sedimentary rocks from the Kaapvaal and Pilbara cratons. Chem. Geol. (in press).

Zhu, X.-K., Guo, Y., O'Nions, R.K., Young, E.D., Ash, R.D., 2001. Isotopic homogeneity of iron in the early solar nebula. Nature 412, 311–313.

Zhu, X.-K., O'Nions, R.K., Guo, Y., Reynolds, B.C., 2000. Secular variation of iron isotopes in North Atlantic Deep Water. Science 287, 2000–2002.